Quantum Effects on Adsorption and Diffusion of Hydrogen and Deuterium in Microporous Materials

A. V. Anil Kumar,[†] Hervé Jobic,[‡] and Suresh K. Bhatia*[,†]

Department of Chemical Engineering, The University of Queensland, Brisbane, QLD 4072, Australia, and Institut de Recherches sur la Catalyse, CNRS, 2 Avenue A. Einstein, 69626 Villeurbanne, France

Received: May 18, 2006; In Final Form: June 29, 2006

Monte Carlo and molecular dynamics simulations and neutron scattering experiments are used to study the adsorption and diffusion of hydrogen and deuterium in zeolite Rho in the temperature range of 30−150 K. In the molecular simulations, quantum effects are incorporated via the Feynman−Hibbs variational approach. We suggest a new set of potential parameters for hydrogen, which can be used when Feynman−Hibbs variational approach is used for quantum corrections. The dynamic properties obtained from molecular dynamics simulations are in excellent agreement with the experimental results and show significant quantum effects on the transport at very low temperature. The molecular dynamics simulation results show that the quantum effect is very sensitive to pore dimensions and under suitable conditions can lead to a reverse kinetic molecular sieving with deuterium diffusing faster than hydrogen.

Introduction

Molecular sieving by microporous materials is one of the methods of separation[1−4] that has many industrial applications, such as in air and hydrocarbon separation, as well as in catalytic processing. When based on equilibrium conditions, molecular sieving relies on the exclusion of large molecule species due to differences between pore diameter and molecular size. However, when this difference is sufficiently small, kinetic molecular sieving, based on differences between diffusivities of the various components, becomes attractive.

Understanding the behavior of adsorbates in microporous materials is essential to the analysis and development of processes involving kinetic molecular sieving. The effects of intermolecular forces, pore confinement, and molecular structure are key to such understanding, as they influence equilibrium and transport behavior while giving rise to many fascinating phenomena such as single file diffusion,[5−7] concerted cluster dynamics,[8] and levitation effects.[9,10] Here, we report on our studies of equilibrium and transport of hydrogen isotopes in a microporous zeolite, with the aim of understanding possible kinetic molecular sieving. While simple and cost-effective, such molecular sieving is conventionally not considered feasible for isotope separation because, from a classical viewpoint, different isotopes of the same element are similar in terms of size and shape as well as energetic considerations. Recently, however, several molecular simulation studies[11−15] have shown selectivity for the heavier isotope, deuterium, over hydrogen when quantum effects become important. Separation processes based on such selectivity can be advantageous over conventional methods for isotope separations such as diffusional separation, laser isotope separation, microwave molecular separation, and cryogenic distillation that are complex and highly energy intensive. Moreover, they have relatively poor selectivity for hydrogen isotope separation.

* To whom correspondence should be addressed. E-mail: sureshb@cheque.uq.edu.au.

[†] The University of Queensland.

[‡] Institut de Recherches sur la Catalyse.

At sufficiently low temperatures, the hydrogen molecule and its isotopes can be no longer treated as classical molecules, as quantum effects are significant at these temperatures due to their low mass, particularly for nanoscale confinements comparable to the de Broglie wavelength. Path integral Monte Carlo simulations and theoretical calculations have shown that the higher mass isotopes are adsorbed preferentially in nanoporous materials such as carbon nanotubes.[11−14] This quantum sieving was first proposed by Beenaker based on their calculations on a simple model of hard spheres in hard cylindrical pores.[16] Later, this was confirmed by many authors using theoretical methods, path integral Monte Carlo simulations, and Monte Carlo simulations using the Feynman−Hibbs variational approach.[11−14] However, all these investigations are confined to the equilibrium adsorption and selectivity of hydrogen isotopes. Recently, we have investigated the quantum effects on the dynamical properties of different hydrogen isotopes in zeolite Rho using molecular dynamics simulations,[15] with quantum corrections incorporated into the classical intermolecular potential using the Feynman−Hibbs variational approach.[17] The results suggested that at sufficiently low temperatures, there exists a quantum induced reverse kinetic sieving in which the heavier isotope diffuses faster than the lighter one through the microporous material. Coupled with higher equilibrium selectivity for the heavier isotope, this counterintuitive finding suggests the possibility of exploiting the low-temperature quantum effect for separation of hydrogen isotopes. In this paper, we report our further investigations of this effect, through quasi-elastic neutron scattering (QENS) experiments and molecular dynamics simulations of diffusion of hydrogen and deuterium in zeolite Rho, and analyze the factors that lead to the reversal of the kinetic selectivity.

Feynman−Hibbs Formalism. The molecular dynamics simulations we describe in this paper use the Feynman−Hibbs variational approach to include quantum effects. In this formalism, a quantum particle of mass m is characterized by a Gaussian, with a width $\sqrt{\beta\hbar^2/12\mu}$ that accounts for the spread

10.1021/jp063034n CCC: $33.50
Published on Web 08/03/2006

in the position due to the uncertainty principle. The quantum partition function of such N particles can be written as[17]

$$Z_{FH} = \frac{1}{N!}\left(\frac{m}{2\pi\beta\hbar^2}\right)^{3N/2}\int \ldots \int dr_1 \ldots dr_N \exp[-\beta\sum_{i<j} U_{FH}(r_{ij})] \quad (1)$$

where $\beta = 1/k_B T$ and

$$U_{FH}(r) = \left(\frac{6\mu}{\pi\beta\hbar^2}\right)^{3/2}\int dR U(|r+R|)\exp\left(-\frac{6\mu}{\beta\hbar^2}R^2\right) \quad (2)$$

$U_{FH}(r)$ is the effective potential between a pair of molecules, with reduced mass μ. The integration in eq 2 is computationally very costly and practically infeasible for a complex potential energy surface as that of zeolite Rho. Moreover, there is a singularity in the pair potential, $U(r)$, at the origin due to the exclusion principle, which causes the integral in eq 2 to diverge. To surmount these difficulties, we expand $U(|r+R|)$ around r to the fourth order in R and substitute in eq 2, which leads to the expression[15]

$$U_{FH}(r) = U(r) + \frac{\beta\hbar^2}{24\mu}\left[U''(r) + \frac{2U'(r)}{r}\right] + \frac{\beta^2\hbar^4}{1152\mu^2}\left[\frac{15U'(r)}{r^3} + \frac{4U'''(r)}{r} + U''''(r)\right] \quad (3)$$

where the prime, double prime, etc. denote the first, second, and higher order derivatives with respect to r. Previous studies on bulk fluids have considered such an expansion, but only up to quadratic terms, and have been found to be accurate enough to predict the thermodynamic and dynamic properties.[18−19] However, this quadratic approximation fails to provide the required accuracy in the case of confined fluids. The quartic approximation to the FH potential in eq 3 appears as the sum of classical pair interaction potential and a perturbation term due to the quantum corrections and was noted to be more accurate than the quadratic approximation. This FH potential can be easily incorporated in the standard molecular dynamics and Monte Carlo simulation programs.

Structure of Zeolite Rho. The zeolite Rho sample used in this investigation was provided by the DuPont Corporation. It has a chemical composition[20] of $D_{5.3}Cs_{0.7}Al_6Si_{42}O_{96}$ with a high Si/Al ratio of 7. At ambient temperature, it crystallizes to the space group $I\bar{4}3m$ with a unit cell dimension $a = 14.8803$ Å. The structure of this zeolite Rho has been reported by Fischer et al. from neutron powder diffraction studies,[20] and the atomic coordinates reported by them have been used to model the host framework in the current simulations. Figure 1 shows the structure of ($2 \times 2 \times 2$) unit cells of zeolite Rho. It must be noted that this zeolite Rho structure is different from that considered in our recent investigation.[15] In our previous calculations, we used a zeolite Rho material with a unit cell composition[21] of $Cs_{1.35}(SiAl)_{48}O_{96}D$, in which the Si/Al ratio was arbitrarily chosen as unity since these atoms were not distinguished in the diffraction experiment. There are two important differences between these two structures: (i) the unit cell dimension increases from 1.4601 to 1.488 nm and (ii) the center-to-center window diameter changes from 0.543 to 0.596 nm. These differences between the two structures are related to the difference in the Si/Al ratio. Increasing the Si/Al ratio decreases the number of cations present in the structure, and the cation size and location play important roles in determining the void structure and dimensions.[22]

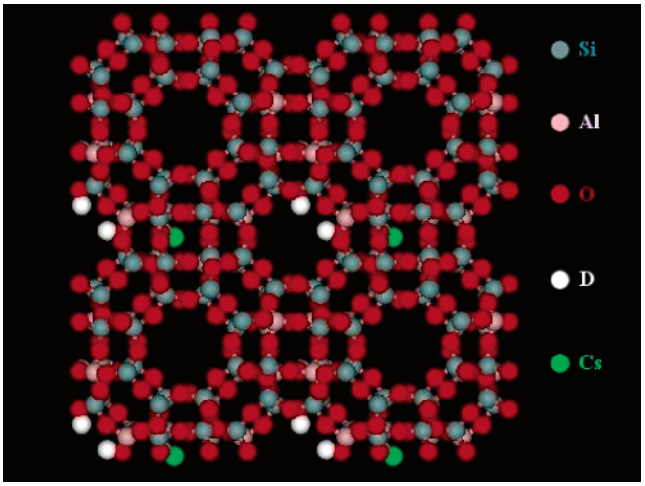

Figure 1. $2 \times 2 \times 2$ unit cells of zeolite Rho structure. The atomic coordinates are taken from ref 20.

Computational Details

In our simulations, we adopted the conventional rigid solid assumption for the host zeolite Rho, neglecting the effects of vibrational motions of the solid atoms around their mean positions. There have been many studies in the literature incorporating the lattice vibrations of host atoms in the diffusion of sorbates, but they remain inconclusive about its importance.[23−25] Moreover, the temperatures at which we conduct the simulations are very low (30−160 K), so that the vibrational motions of the solid atoms can be ignored.

Grand canonical Monte Carlo (GCMC) simulations were performed to model the equilibrium properties of bulk hydrogen molecules and the hydrogen adsorption in zeolite Rho. GCMC simulations can provide the average values of the state point variables of bulk hydrogen, which in turn can test the accuracy of intermolecular potential parameters or determine new potential parameters. By specifying the chemical potential and temperature of the confined system, GCMC can determine the amount adsorbed in the case of the confined systems. The GCMC method consists of the moves for displacement, creation, and deletion in the simulation box, which will be accepted or rejected according to the particular probability for each of these moves. In both creation and deletion moves, microscopic reversibility is ensured by having an equal number of creation and deletion moves.

Canonical ensemble molecular dynamics simulations were used to investigate the dynamic properties of hydrogen and deuterium in zeolite Rho. The underlying idea behind molecular dynamics simulations is to solve Newton's equations of motion numerically, and the evolving trajectory of the system is used to calculate the average dynamical properties of the system. The temperature is constantly maintained by using a Gaussian thermostat, described by Evans and Moriss.[26] A time step of 1 fs is used in all the simulations. Each simulation run is comprised of 20 ns, of which the initial 5 ns trajectory is ignored in the calculations of dynamical properties. The self-diffusivity and transport diffusivity are calculated from the single particle and center of mass mean squared displacement, respectively, using the Einstein equation[27]

$$D = \lim_{t\to\infty}\frac{\langle|\Delta r|^2(t)\rangle}{6t} \quad (4)$$

The 15 ns run period during which the dynamics properties are

determined has been split into five smaller runs to calculate the error involved in the estimation of transport properties.

Experimental Procedures

Adsorption Isotherm. The adsorption isotherm was measured volumetrically on a homemade instrument. The gas pressure was recorded with a MKS Baratron capacitive sensor. The zeolite Rho was activated in a glass cell on a vacuum line by slow heating to 643 K, and the cell was then connected to the volumetric apparatus. To measure the isotherm at 80 K, the adsorption cell was plunged into liquid nitrogen, whose level was kept constant during the experiment.

Quasi-Elastic Neutron Scattering. The quasi-elastic neutron scattering experiments were performed on the spectrometer IN6, at the Institut Laue-Langevin, Grenoble, France. The incident neutron energy was taken as 3.12 meV, corresponding to a wavelength of 5.1 Å. Spectra were recorded at various scattering angles, corresponding to wave vector transfers, Q, ranging from 0.28 to 1.53 $Å^{-1}$. Spectra from different detectors were grouped to obtain reasonable counting statistics and to avoid the Bragg peaks of the zeolite. The line shape of the elastic energy resolution could be fitted by a Gaussian function, whose full width at half-maximum (fwhm) varied from 82 μeV at a small Q value to 105 μeV at a large Q value.

Since the hydrogen atom has the largest neutron cross-section, the degassed zeolite Rho was exposed to D_2O vapor at about 470 K, two times, to exchange the protons from the zeolite by deuterium atoms. The sample was then dehydrated by pumping under slow heating to 643 K (final pressure better than 10^{-3} Pa). The zeolite was transferred inside a glovebox into a slab-shaped aluminum container, which could be connected to a gas inlet system allowing in situ adsorption. After recording the scattering of the dehydrated zeolite, two concentrations of H_2 and D_2 (1.4 and 2.8 molecules per cage, on average) were studied at various temperatures. The loadings were determined from the equilibrium pressures and from the measured adsorption isotherm.

H_2 is essentially an incoherent scatterer, allowing the determination of the self-diffusivity. D_2 is both incoherent and coherent, so that in principle, both the self- and transport diffusion coefficients can be determined,[28] but at low loading, these two diffusivities should have the same values.

Results and Discussion

Potential Parameters. The fluid−fluid and fluid−zeolite interactions are modeled by the (12−6) Lennard-Jones (LJ) potential in the simulations. In our previous investigation, we have used the Buch parameters to model the H_2-H_2 interactions. These parameters were originally proposed by Michels et al. by fitting the experimental gas-phase isotherms of hydrogen and deuterium in the temperature range from −175 to 150 °C.[29] It is to be noted that they have obtained slightly different parameters for hydrogen and deuterium that are not expected classically. It may be argued that the difference in the values of the LJ energy parameter, ϵ/k_B, and the interaction length scale parameter, σ, for hydrogen and deuterium is due to quantum effects. Subsequently, Buch modified these parameters slightly, to obtain better agreement with the mean potential energies of the D_2 clusters.[30] Here, we have carried out GCMC simulations to determine whether these parameters reproduce bulk hydrogen data[31,32] when the quantum effects are included explicitly. The results are shown in Figures 2 and 3. The line corresponds to the experimental data and the squares to the results obtained from GCMC simulations using the Buch parameters. As can be seen from the figures, the state points obtained from simulations deviate from the corresponding experimental data. To improve the potential parameters, we performed several GCMC simulations of bulk hydrogen at different state points while using different interaction parameters for the H_2-H_2 interactions to obtain agreement with the data. The best fitted parameters are $\sigma_{H_2-H_2} = 0.2782$ nm and $\epsilon_{H_2-H_2}/k_B = 38.7$ K. The variation of bulk pressure and of the density of H_2 with fugacity at 77 K, using these parameters, is given in Figure 2. The simulation results are in excellent agreement with the experimental data[31] for the previous parameter values. We also compared the densities at different temperatures where the experimental data[32] are available, which support the validity of the new parameters. This is shown in Figure 3. A higher value for the interaction strength $\epsilon_{H_2-H_2}/k_B$ and a lower value for $\sigma_{H_2-H_2}$ as compared to the Buch parameters are understandable since the quantum effects (overlooked in the Buch estimations) tend to reduce the well depth and increase the length parameter.

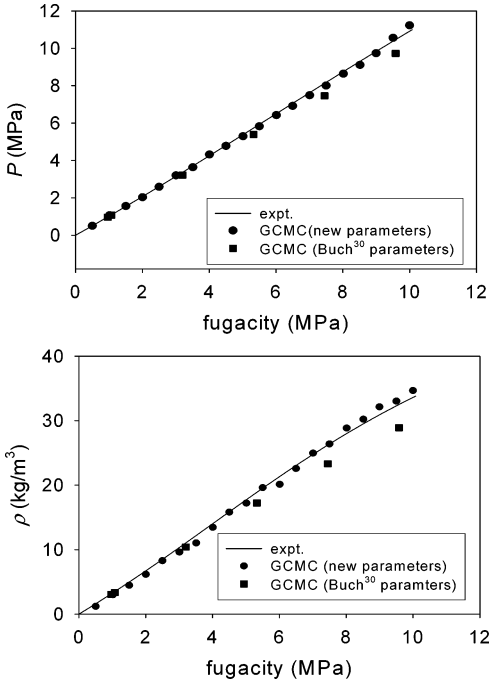

Figure 2. Pressure and density of bulk H_2 at different fugacities. The solid line corresponds to the experimental results[31] and the symbols to GCMC simulations.

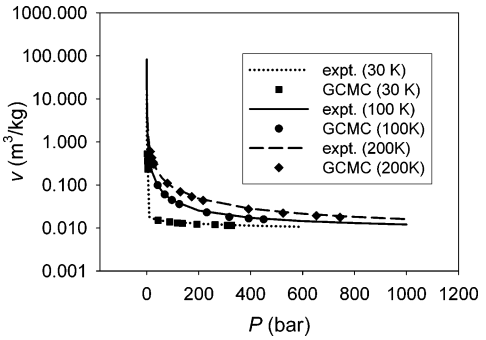

Figure 3. Specific volume of bulk H_2 vs pressure at different temperatures. The lines correspond to experimental values[32] and the symbols to GCMC simulations using the newly obtained potential parameters.

Adsorption Isotherm. We next studied the equilibrium adsorption of H_2 in zeolite Rho. The experimentally obtained isotherm is used to obtain the LJ parameters for the solid−fluid interactions. The best fit obtained from the GCMC

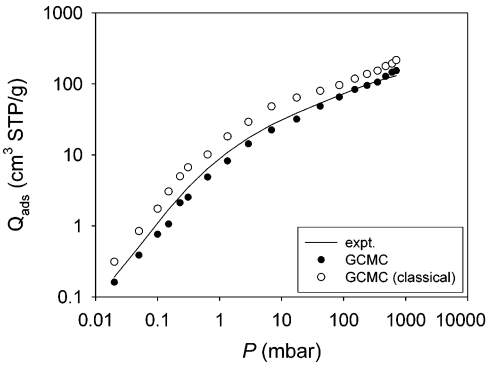

Figure 4. Hydrogen adsorption isotherm in zeolite Rho at 80 K. The solid line is the experimentally obtained isotherm, and the closed symbols are from GCMC simulations. Open symbols represent the adsorption isotherm obtained from GCMC simulations when quantum corrections are neglected.

TABLE 1: Lennard-Jones Potential Parameters for Solid−Solid Interactions

	σ (nm)	ϵ/k_B (K)
O−O	0.2644	165.02
D−D	0.2762	9.1954
Cs−Cs	0.4959	336.639

simulations has been shown in Figure 4 along with the experimental results. The potential parameters thus obtained are given in Table 1 and are very similar to those reported in the literature.[24,33] We have not included the electrostatic interactions in our calculations (for both fluid−fluid and fluid−solid interactions), which may result in higher effective values for the LJ energy parameters. Following the common procedure,[34] we have not included the interactions between the adsorbate and the Si/Al atoms in the solid framework. The Si and Al atoms in the zeolite framework are largely shielded by surrounding oxygen atoms, thus making the short range dispersive interactions of these with the adsorbates insignificant. In Figure 4, we have also plotted the adsorption isotherm obtained from GCMC simulations (open symbols) using these parameters and switching off the quantum corrections. The results clearly demonstrate that the quantum effects reduce the equilibrium adsorption, as suggested also by path integral Monte Carlo simulations.[11−14] However, at 80 K, the effect on equilibrium, while not insignificant, is small.

Diffusion and Transport. The QENS spectra obtained for H_2 at the first loading and at the lowest wave vector transfer are shown in Figure 5. The larger the broadening of the spectra, the faster is the diffusion. At this wave vector transfer value, 0.28 $Å^{-1}$, the length scale probed is 22 Å, so that one is following long-range translation, corresponding to cage-to-cage motion. The spectra were first fitted individually with a Lorentzian function, corresponding to the diffusion motion, convoluted with the instrumental resolution. The spectra were then fitted simultaneously using a jump diffusion model, to extract a diffusion coefficient.

Using the parameters obtained in the previous sections, we have carried out NVT ensemble molecular dynamics simulations to study the dynamics properties of H_2 and D_2 in zeolite Rho. The results obtained from the simulations have been compared with those from neutron scattering experiments. The temperature variations of the self-diffusivities of H_2 and D_2 at a density of 1.4 molecules per unit cell have been plotted in Figure 6. The closed symbols correspond to the neutron scattering data and the open symbols to the molecular dynamics simulation results. The results from the two methods are in excellent agreement

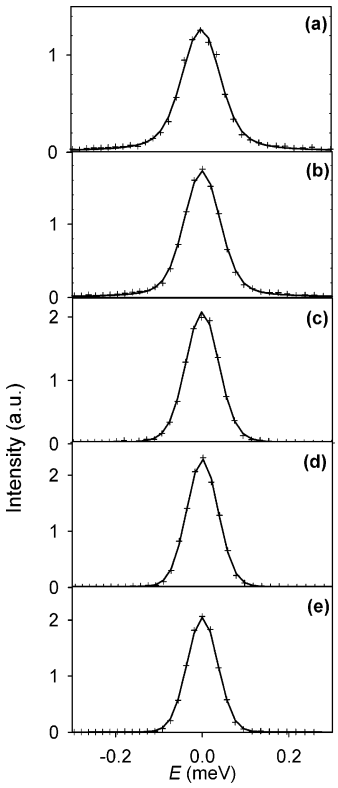

Figure 5. Comparison between experimental (crosses) and calculated (solid lines) QENS spectra obtained for H_2 in zeolite Rho at different temperatures: (a) 140 K, (b) 120 K, (c) 100 K, (d) 77 K, and (e) 50 K ($Q = 0.28$ $Å^{-1}$, loading: 1.4 molecules per cage).

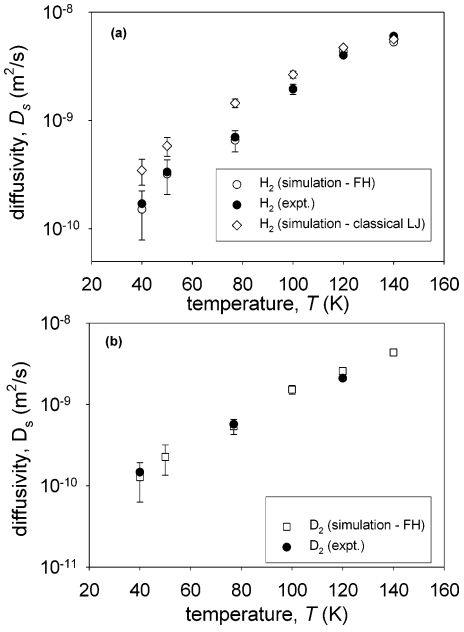

Figure 6. (a) Variation of diffusivity of H_2 (circles) in zeolite Rho with temperatures at a density of 1.4 molecules per unit cell. The MD simulation results for H_2 using the classical Lennard-Jones potential are also shown (diamonds). (b) Diffusivity variation of D_2 (squares) in zeolite Rho. In all cases, the closed symbols correspond to experimental results and open symbols to equilibrium MD simulations.

with each other. Also shown in the figure is the result for hydrogen based on the classical LJ interaction model, neglecting quantum effects. While the classical results match the experimental data at temperatures above about 100 K, below this temperature they predict significantly higher diffusivities, and the simulations considering the quantum effect match the

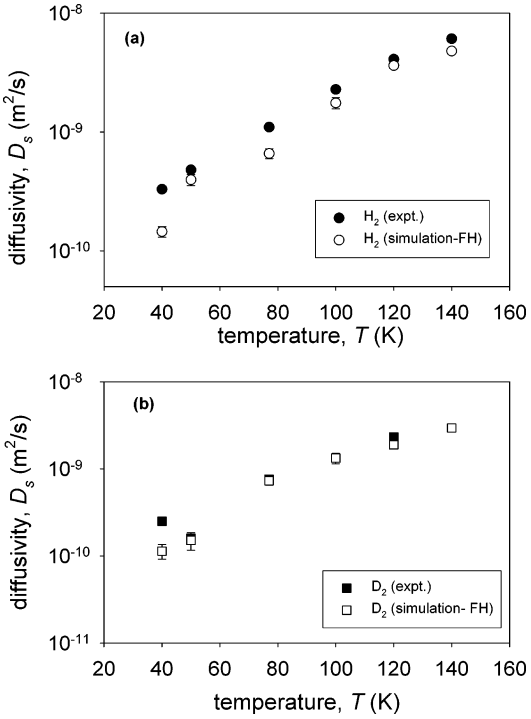

Figure 7. Temperature variation of the diffusivity of (a) H_2 (circles) and (b) D_2 (squares) in zeolite Rho, at a density of 2.8 molecules per unit cell. The closed symbols correspond to the values obtained from the neutron scattering experiments and open symbols to equilibrium MD simulations.

experimental data much more closely. These results confirm the importance of quantum effects below about 100 K. Here, we do not observe a reverse kinetic sieving, noted in our previous investigation.[15] The zeolite structure used in the present investigations has a larger window diameter, which is too big to block the cage-to-cage migration at low temperatures. Thus, the effective increase in the diameter of H_2 molecules at low temperatures due to the quantum effects is not sufficiently large to localize it by blocking its migration from one cage to another through the window. Consequently, the diffusivity of H_2 does not decrease sharply in the temperature range studied, and there is no significant kinetic selectivity for deuterium for the zeolite Rho used here. Nevertheless, as shown next, our studies show that quantum effects at low temperatures are significant for lighter particles such as H_2 and D_2, and a high selectivity for D_2 can be obtained if we carefully choose the host material. Figure 7 shows the temperature variation of the diffusivities of H_2 and D_2 at a density of 2.8 molecules per unit cell. As before, the closed symbols are from the neutron scattering experiments and open symbols from the molecular dynamics simulations. In this case also, the diffusivity values obtained from MD simulations and neutron scattering experiments are in good agreement with each other.

Using the new parameters, we have carried out molecular dynamics simulations of H_2 and D_2 in the structure of zeolite Rho used in our previous calculations.[15] This zeolite structure has a smaller window (0.543 nm), which may play a role in the reversal of kinetic selectivity. We have analyzed the trajectories obtained from these simulations and calculated the diffusion coefficients at various temperatures. Here, the density of the sorbates was one molecule per the alpha cage of the zeolite Rho, and at this low density, the self-and transport diffusivities are essentially equivalent. However, the transport diffusivity is more pertinent for selectivity and flux calculations and is the quantity considered here. Figure 8 depicts the results.

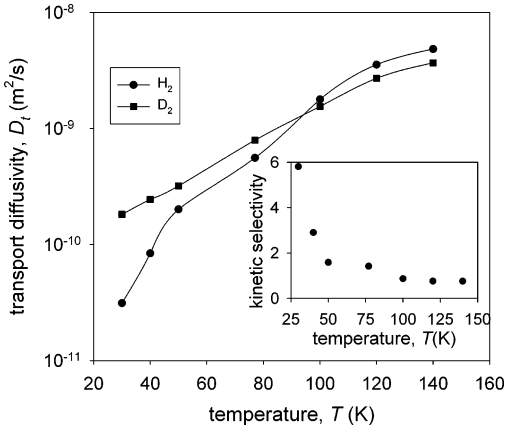

Figure 8. Temperature variation of the transport diffusivity of H_2 and D_2 in zeolite Rho having a narrower window. D_2 begins to diffuse faster in this structure around 94 K. The kinetic selectivity of D_2 over H_2 at various temperatures is shown in the inset.

At high temperatures, we observe that H_2 diffuses faster than D_2. However, as the temperature decreases, the ratio between the diffusivity of D_2 to that of H_2 increases, and at approximately 94 K, D_2 begins to diffuse faster than H_2. Around this temperature, H_2 molecules feel the steric hindrance for the cage-to-cage migration, and its diffusivity starts decreasing at a rapid rate, while the deuterium can still pass through the window from one cage to another without much difficulty. Upon decreasing the temperature further, the kinetic selectivity of D_2 increases, and at 30 K, it reaches a value of 5.81. The kinetic selectivity at different temperatures is shown as the inset in Figure 8. This reversal of kinetic selectivity due to quantum effects, first reported by us in an earlier paper,[15] is supported by the recent experimental work of Zhao et al.[35] These authors report the experimental verification of this kinetic isotope effect for H_2 and D_2 in porous carbon molecular sieves with micropore dimension of 0.546 and 0.566 nm, similar to the smaller window (0.543 nm) zeolite Rho, wherein H_2 shows a slower adsorption/desorption kinetics than D_2 at 77 K. Based on Figure 8, we anticipate that the crossover of the diffusivities occurs at about 94 K, so that the faster diffusion of D_2 at 77 K, observed by Zhao et al.,[35] is expected given their similar pore size.

These investigations point toward the importance of the pore dimension in achieving the reverse kinetic selectivity. We do not observe the reversal of kinetic selectivity in the zeolite Rho structure examined here, where the window diameter is 0.596 nm, while we do predict quantum mediated reverse kinetic selectivity for D_2 for the structure where the window diameter is 0.543 nm. A difference of 0.05 nm in the pore dimensions results in vastly different dynamic behavior. This shows that the reverse kinetic selectivity is highly sensitive to the pore dimensions and highlights the need to choose the host material judiciously for practical applications.

We have also carried out GCMC simulations of adsorption of hydrogen and deuterium in the structure of zeolite Rho having the narrower (0.543 nm) window, to calculate the equilibrium selectivity. The low pressure isobar at different temperatures is plotted in Figure 9a. From the figure, it is evident that heavier deuterium is adsorbed more strongly than lighter hydrogen in the temperature range studied. Moreover, the difference in the amount adsorbed increases with a decrease in temperature. The equilibrium selectivity of deuterium over hydrogen at these temperatures is plotted as the inset in Figure 9a. The equilibrium selectivity increases as the temperature decreases and is 3.9 at 30 K. These observations are in agreement with earlier

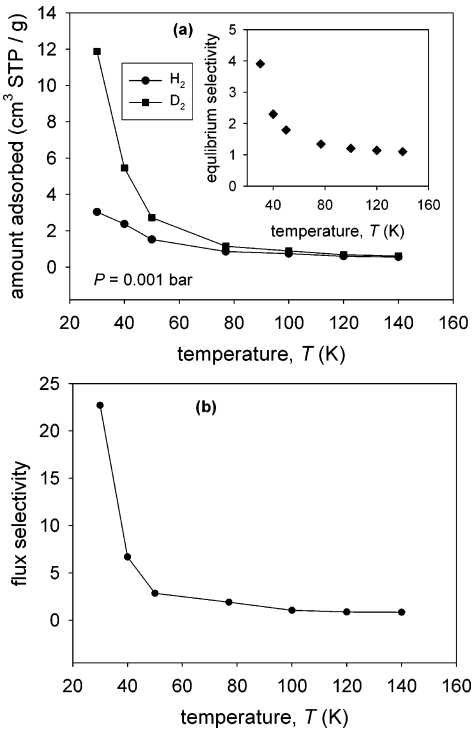

Figure 9. (a) Adsorption isobars of hydrogen and deuterium in zeolite Rho plotted against temperature. The equilibrium selectivity is shown in the inset. (b) Temperature variation of flux selectivity of deuterium over hydrogen in zeolite Rho at low pressure.

investigations of the equilibrium adsorption of hydrogen isotopes in nanopores.[11−14]

The equilibrium and kinetic selectivities obtained previously suggest the feasibility of zeolite Rho supported membrane separation of hydrogen isotopes. Rather than the kinetic selectivity or equilibrium selectivity, it is the product of the two that gives the ratio of the fluxes, which indicates the potential of such membrane separation. In Figure 9b, we have plotted the variation of this flux selectivity with temperature. At higher temperatures, the flux selectivity is rather low; however, at lower temperatures, it increases and reaches an attractive value of 22.66 at 30 K. These results suggest that a new separation process exploiting the quantum effects due to low temperature, light mass, and narrow confinement may be a promising candidate for replacing the energy expensive conventional processes for hydrogen isotope separation.

Conclusion

To summarize, we have obtained a new set of LJ parameters of H_2-H_2 interactions, which can be employed with Feynman−Hibbs formalism to obtain the bulk physical properties of hydrogen molecules. These parameters are used in molecular dynamics simulations to obtain the diffusivities of H_2 and D_2 in zeolite Rho at low temperatures. The results from MD simulations are in excellent agreement with those from neutron scattering experiments. Our calculations indicate the extreme sensitivity of the reverse kinetic selectivity, observed previously, on the pore dimensions and suggest the possibility of separation at very low temperatures in suitable materials.

Acknowledgment. This research has been supported by a Discovery Grant from the Australian Research Council. The neutron experiments were carried out at the Institut Laue-Langevin, Grenoble, France. We thank this Institute for the allocation of beam time and Dr. H. Schober for his help during the measurements. The authors are grateful to Dr. David Corbin, DuPont Research Station, Wilmington, for providing the sample of the zeolite Rho utilized here.

References and Notes

(1) Karger, J.; Ruthven, D. M. *Diffusion in Zeolites and Other Microporous Solids*; Wiley-Interscience: New York, 1992.
(2) Bates, S. P.; van Santen, R. A. *Adv. Catal*. **1998**, *42*, 1−114.
(3) Breck, D. W. *Zeolite Molecular Sieves*; John Wiley and Sons: New York, 1974.
(4) Yang, R. T. *Adsorbents: Fundamentals and Applications*; Wiley-Interscience: New York, 2003.
(5) Hahn, K.; Karger, H.; Kukla, V. *Phys. Rev. Lett*. **1996**, *76*, 2762−2765.
(6) Kukla, V.; Kornatowski, J.; Demuth, D.; Girnus, I.; Pfefier, H.; Rees, L. V. C.; Schunk, S.; Unger, K. K.; Karger, H. *Science* **1996**, *272*, 702−704.
(7) Jobic, H.; Hahn, K.; Kärger, J.; Bée, M.; Tuel, A.; Noack, M.; Girnus, I.; Kearley, G. J. *J. Phys. Chem. B* **1997**, *101*, 5834−5841.
(8) Sholl, D. S.; Fichthorn, K. A. *Phys. Rev. Lett*. **1997**, *79*, 3569−3572.
(9) Santikary, P.; Yashonath, S. *J. Phys. Chem*. **1994**, *98*, 6368−6376.
(10) Kumar, A. V. A.; Bhatia, S. K. *J. Phys. Chem. B* **2006**, *110*, 3109−3113.
(11) Wang, Q. Y.; Challa, S. R.; Sholl, D. S.; Johnson, J. K. *Phys. Rev. Lett*. **1999**, *82*, 956−959.
(12) Challa, S. R.; Sholl, D. S.; Johnson, J. K. *Phys. Rev. B* **2001**, *63*, 245419.
(13) Challa, S. R.; Sholl, D. S.; Johnson, J. K. *J. Chem. Phys*. **2002**, *116*, 814−824.
(14) Tanaka, H.; Kanoh, H.; El-Merraoui, M.; Steele, W. A.; Yudaska, M.; Iijima, S.; Kaneko, K. *J. Phys. Chem. B* **2004**, *108*, 17457−17465.
(15) Kumar, A. V. A.; Bhatia, S. K. *Phys. Rev. Lett.* **2005**, *95*, 245901.
(16) Beenakker, J. J. M.; Borman, V. D.; Krylov, S. Y. *Chem. Phys. Lett*. **1995**, *232*, 379−382.
(17) Feynman, R. P.; Hibbs, A. R. *Quantum Mechanics and Path Integrals*; McGraw-Hill: New York, 1965.
(18) Guillot, B.; Guissani, Y. *J. Chem. Phys*. **1998**, *108*, 10162−10174.
(19) Tchouar, N.; Ould-Kaddour, F.; Levesque, D. *J. Chem. Phys*. **2004**, *121*, 7326−7331.
(20) Fischer, R. X.; Baur, W. H.; Shannon, R. D.; Staley, R. H.; Abrams, L.; Vega, A. J.; Jorgensen, J. D. *Acta Crystallogr., Sect. B* **1988**, *44*, 321−334.
(21) Parise, J. B.; Abrams, L.; Gier, T. E.; Corbin, D. R.; Jorgenson, J. D.; Prince, E. *J. Phys. Chem.* **1984**, *88*, 2303−2307.
(22) Szostak, R. *Molecular Sieves*; Blackie Academic and Professional: London, 1998.
(23) Kopelevich, D. I.; Chang, H.-C. *J. Chem. Phys*. **2001**, *114*, 3776−3789.
(24) Demontis, P.; Suffritti, G. B.; Fois, E. S.; Quartieri, S. *J. Phys. Chem*. **1992**, *96*, 1482−1490.
(25) Fritzsche, S.; Wolfsberg, M.; Haberlandt, R.; Demontis, P.; Suffriti, G. B.; Tilocca, A. *Chem. Phys. Lett.* **1998**, *296*, 253−258.
(26) Evans, D. J.; Morriss, G. P. *Statistical Mechanics of Nonequilibrium Liquids*; Academic: London, 1990.
(27) Allen, M. P.; Tildesley, D. J. *Computer Simulation of Liquids*; Oxford University Press: New York, 1987.
(28) Jobic, H.; Kärger, J.; Bée, M. *Phys. Rev. Lett.* **1999**, *82*, 4260−4263.
(29) Michels, A.; de Graaff, W.; Ten Seldam, C. A. *Physica* **1960**, *26*, 393−408.
(30) Buch, V. *J. Chem. Phys*. **1994**, *100*, 7610−7629.
(31) Younglove, B. A. *J. Phys. Chem. Ref. Data 1982*, *11*, Suppl. 1, 1−349.
(32) *Perry's Chemical Engineers' Handbook*, 7th ed; Perry, R. H., Green, D. W., Eds.; McGraw-Hill: New York, 1998.
(33) Kiselev, A. V.; Du, P. Q. *J. Chem. Soc., Faraday Trans.* **1981**, *77*, 1−15.
(34) June, R. L.; Bell, A. T.; Theodorou, D. N. *J. Phys. Chem*. **1991**, *95*, 8866−8878.
(35) Zhao, X.; Villar-Rodil, S.; Fletcher, A. J.; Thomas, K. M. *J. Phys. Chem. B* **2006**, *110*, 9947−9955.